GEOPHYSICAL RESEARCH LETTERS, VOL. 34, L23307, doi:10.1029/2007GL031454, 2007

Power-law distribution of fault slip-rates in southern California

Brendan J. Meade[1]

Received 31 July 2007; revised 19 October 2007; accepted 31 October 2007; published 8 December 2007.

[1] The spatial partitioning of deformation in the continental crust and, in particular, at plate boundary zones is determined by the distribution of fault slip-rates. Analytic and numerical models of strain accumulation in the elastic upper crust have been divided into those that parameterize faulting as localized on a finite length fault system comprised of relatively few fast slip-rate faults, or as distributed throughout a continuum of relatively slow slip-rate faults. We demonstrate that in the southern California fault system, between the Pacific and North American plates, both geologically and geodetically constrained fault slip-rate catalogs obey a power-law frequency distribution. Using this empirically constrained scaling relationship we derive an analytic expression for the partitioning of potency accumulation rate, which determines the distribution and magnitude of slip localization. This model describes the kinematics of both micro-plate and continuum deformation models, and predicts that ~97% of the deformation in southern California is accommodated on faults slipping at >1 mm/yr which is consistent with models of continental deformation which explicitly represent a large though finite number of deforming structures. **Citation:** Meade, B. J. (2007), Power-law distribution of fault slip-rates in southern California, *Geophys. Res. Lett.*, *34*, L23307, doi:10.1029/2007GL031454.

1. Introduction

[2] Our understanding of continental tectonics, and the spatial pattern of deformation at plate boundary zones, has evolved since the plate tectonics revolution to include both continuum models of distributed faulting [e.g., *England and Molnar*, 1997; *Molnar*, 1988] and micro-plate models of finite length fault systems [e.g., *McCaffrey*, 2002]. These two end member models differ in their treatment of deformation between major faults and, in particular, what role a potential continuum of relatively slow slip-rate faults might play in a highly fractured crust [*England and McKenzie*, 1982; *Molnar*, 1988; *Thatcher*, 1995]. Determining the limits of applicability for these models has remained difficult due to lack of an empirically constrained model of fault slip-rate distributions that would enable the quantification of slip localization. The frequency distribution of continental fault slip-rates also spans a gap in crustal deformation scaling models. Over coseismic time scales (10^0–10^3 seconds), power-law relationships between rupture length, slip, and magnitude have been constrained by regressing observations from ~70 $M_W \geq 5.5$ earthquakes [*Hanks and Bakun*, 2002; *Wells and Coppersmith*, 1994]. Over geologic time scales (10^4–10^6 years), the integrated effects of faulting and fracturing have produced power-law relationships between fault length and accumulated slip at both the outcrop and plate boundary scale [e.g., *Cowie and Scholz*, 1992; *Marrett and Allmendinger*, 1992]. Here we describe an empirical scaling relationship for fault slip-rates, which provides a quantitative framework describing continental deformation spanning both coseismic and geologic time scales.

[3] To characterize both the mean kinematic behavior and the spatial pattern of deformation at plate boundary zones we analyze fault slip-rates in southern California where the relative motion between the Pacific and North American plates is accommodated across a plate boundary zone ~200 km wide [e.g., *Petersen and Wesnousky*, 1994]. In this locale, geologically and geodetically constrained slip-rate estimates are uniquely dense, allowing for the empirical determination of the relative role of slip both on and off of major faults. Efforts to integrate fault slip-rates into kinematically consistent models of the southern California fault system that match far-field plate motion constraints [*Meade and Hager*, 2005; *Minster and Jordan*, 1987; *Weldon and Humphreys*, 1986] have led to the identification of the "San Andreas deficit" where <70% of the ~50 mm/yr of relative motion between the Pacific and North American plates [*DeMets et al.*, 1990; *DeMets and Dixon*, 1999] is accommodated on the San Andreas fault [*Minster and Jordan*, 1987]. Geodetic measurements, averaged over 3–15 year intervals, have been used to identify additional zones of active faulting in southern California, including the Eastern California Shear Zone, which accommodates 10–15 mm/yr of motion [*McClusky et al.*, 2001; *Sauber et al.*, 1994]. Estimating fault slip-rates from geodetic data requires a model for the elastic behavior of the upper crust to account for near fault velocity gradients resulting from interseismic elastic strain accumulation [*Savage and Burford*, 1973]. The two methods for modeling for this effect are to either explicitly represent the elastic strain accumulation associated with the motion of individual faults [e.g., *Argus and Gordon*, 2001; *Bennett et al.*, 1996; *Bennett et al.*, 1997; *Fay and Humphreys*, 2005; *Feigl et al.*, 1993; *McClusky et al.*, 2001; *Meade and Hager*, 2005] or to parameterize regions of complex faulting with continuous velocity gradients as a proxy for deformation on a large number of relatively slow slip-rate faults [e.g., *Billen and Houseman*, 2004; *Bourne et al.*, 1998; *Flesch et al.*, 2000; *Shen-Tu et al.*, 1999]. While the first method allows for the direct estimation of fault slip-rates inferred from models of interseismic strain accumula-

[1]Department of Earth and Planetary Science, Harvard University, Cambridge, Massachusetts, USA.

0094-8276/07/2007GL031454$05.00

tion, the second method does not, due to the composite nature of deforming regions.

2. Observational Constraints on the Frequency Distribution of Fault Slip-Rates

[4] In this paper we analyze fault slip-rates from two independent southern California slip-rate catalogs: (1) a compilation of geologic estimates, and (2) those inferred from a geodetically constrained model of interseismic behavior in the elastic upper crust where deformation is explicitly partitioned on specific structures. Geologically derived slip-rates, based on the displacement rates of offset marker units averaged over Holocene to Quaternary intervals, have been compiled for southern California for ~6900 km of fault system length (Figure 1a) and provide constraints on the long-term behavior of the fault system [*Petersen and Wesnousky*, 1994]. Long-term fault slip-rate estimates are complemented by models based inferences of present day slip-rates models of earthquake cycle activity and constrained by Global Positioning System observations. Geodetically constrained slip-rate estimates were derived from a kinematically consistent, elastic block model of the southern California fault system composed of 24 rotating micro-plates and ~5700 km of contiguous fault system (Figure 1b) [*Meade and Hager*, 2005]. The geologic and geodetic slip-rate catalogs similarly constrain the Central San Andreas fault slip-rate at 34–36 mm/yr while they differ considerably for some faults in the Eastern California Shear Zone where geodetic rates are faster than geologic rates for the Blackwater fault but slower for the Garlock fault [*McClusky et al.*, 2001; *Meade and Hager*, 2005].

[5] Both southern California fault slip rate catalogs indicate that the majority of the fault system moves at relatively slow slip-rates, <5 mm/yr, and that fast slip-rates, >10 mm/yr, are localized on the San Andreas and San Jacinto faults (Figures 1a and 1b). The relative partitioning of fast and slow slip-rate faults can be described in terms of their frequency distribution, by quantifying the fraction of a fault system moving at a given slip-rate. To calculate the fault slip-rate frequency distribution and account for the estimated lengths of faults we divide all faults (ranging in length from 2–350 km), along strike, into segments with a uniform length of 1 km, assigning the same slip-rate to all segment of a given fault. This discretization eliminates an arbitrary choice of fault endpoints in the kinematically consistent slip-rate models. The frequency distribution of normalized fault slip-rates, $v = |v_{obs}/v_{max}|$, (where v_{max} is the maximum slip-rate in the fault system) can be described by a power-law of the form,

$$N(v) = cv^{\theta} \tag{1}$$

where $N(v)$ is the number fault segments moving at slip-rate v, c is a coefficient of proportionality, and θ is the power-law exponent. The power-law exponent can be interpreted in terms of the relative fraction of the fault system at relatively fast and slow slip-rates. Values of $\theta > 0$ and $\theta < 0$ correspond to slip-rate distributions where relatively slip rates >0.5 v_{max} and <0.5 v_{max} respectively, constitute the majority of the observed length of the fault system, while there is white distribution of slip-rates for the $\theta = 0$ case. The geologically and geodetically constrained fault slip-rate catalogs can be described by negative power-law exponents of $\theta_{geol} = -0.79 \pm 0.13$ and $\theta_{geod} = -0.64 \pm 0.07$, quantifying the observation that most of the southern California fault system is characterized by relatively slow slip-rate faults (Figures 1c and 1d). Throughout the rest of this paper, we use a composite power-law exponent equal the mean value of the range of values spanned by the geologic and geodetic estimates and their uncertainties, $\theta = -0.75 \pm 0.18$. The power-law exponent uncertainty estimates were determined by calculating the standard deviation of the estimated value of θ as a function of variable binning intervals. Estimates of θ vary by as much as a factor of two for frequency distributions constructed with fewer than 20 bins while there is ~10% variation when the number of bins exceeds 20 (Figures 1c and 1d). Because the same slip-rate is used for all segments of a fault there is no dependence on the discretization length scale used to calculate the frequency distribution, with the exception of truncation errors at fault tips.

[6] That the geodetically inferred frequency distribution exponent is smaller than the geologic one is likely due to the fact that very slow slip-rate faults (<1 mm/yr) are poorly represented in this model (Figures 1b and 1d). In other words, deformation associated with very slow slip-rate faults may be under-represented in current micro-plate models of southern California and may have been artificially mapped on other structures [*McCaffrey*, 2005; *Meade and Hager*, 2005]. An example of this aliasing is the observation that the slowest slip rate bin in Figure 1d has fewer segments that the next two at slightly greater values. This appears as a change in the sign of the slope of the frequency distribution as the block model fault slip rates approach 0 mm/yr and increase in the magnitude of the slope for those faults slipping in excess of 3 mm/yr. The effect of this low slip rate aliasing may be quantified by developing fault system models that incorporate more individual structures and greater fault system length [e.g., *Plesch et al.*, 2007].

[7] It may also be possible to describe the fault slip-rate frequency distribution as lognormal, where the number of faults decreases as the slip-rate approaches 0 mm/yr. Such a model would not be scale-independent, and would preclude any significant contribution to the overall deformation budget from very slow slip-rate faults (e.g., <1 mm/yr) due to the simple fact that there would be so few. It is also conceivable that the frequency of very slow slip-rate faults increases at very slow slip-rates. However this supposition is not observed at the scale of presently available slip-rate observations and we are not aware of any mechanical models that predict a break of this sort at very slow slip-rates.

3. Implications for Fault System Length and Potency Partitioning

[8] The empirically constrained power-law fault slip-rate distribution can be used to calculate both the total fault system length and potency accumulation rate of the southern California fault system. The length of the fault system between two normalized fault slip-rates (v_1, v_2) is given by the integral of the frequency distribution between the two slip-rates, $L = \int_{v_1}^{v_2} N(v)dv = c(v_2^{\theta+1} - v_1^{\theta+1})/(\theta + 1)$, for $\theta > -1$. Assuming that faults at very slow slip-rates obey the

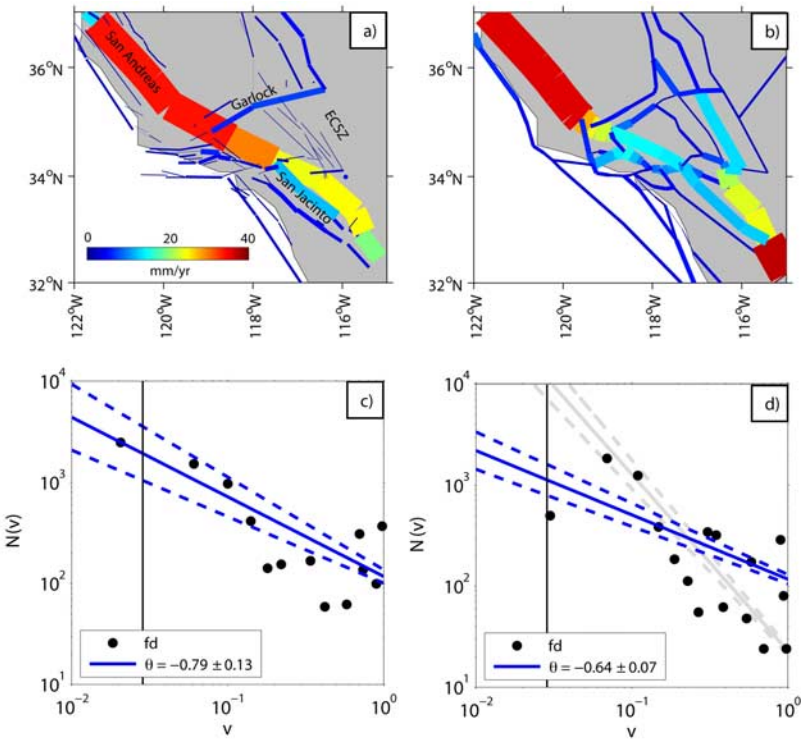

Figure 1. Slip-rate magnitudes and frequency distributions in southern California. Wider lines and reddish tones denote faster slip-rates. (a) Geologically constrained slip-rate estimates and names of selected faults. ECSZ is short for Eastern California Shear Zone. (b) Slip-rates constrained by geodetic data and estimated using a kinematically consistent elastic block model. (c) Black circles show the observed frequency distribution (fd) and the blue line shows the best-fit power-law model. The best-fit to the geologically constrained slip-rate frequency distribution is $\theta_{geol} = -0.79 \pm 0.13$. (d) Frequency distribution best-fit power-law from geodetically constrained elastic block model, $\theta_{geol} = -0.64 \pm 0.07$. The light gray lines show the best fit if the lowest magnitude slip-rate bin observation is ignored. All fault slip-rates, ν, are normalized by the maximum observed slip-rate (~35 mm/yr).

same statistics as those that are observable with current geodetic methods [e.g., *Friedrich et al.*, 2003], we can integrate to obtain the total length of the fault system between any two slip-rates. Fault slip-rates can be normalized over the interval (0,1) by dividing by the maximum slip-rate, v_2. Integrating over all slip rates from v_2 to 0 mm/yr, the total length of the fault system is, $L = c/(\theta + 1)$. As θ approaches -1 the length of the faults system at slow slip-rates increases relative to that at fast faults and the total length of the fault system diverges (Figure 2a). In southern California, with $\theta \cong -0.75$, faults slipping at rates between 1 and 35 mm/yr constitute ~67% of the total fault system length while those slipping <1 mm/yr contribute the remaining ~33%. There is a roughly equal partitioning between the length of the fault system slipping at <1, 1–10, and >10 mm/yr rates.

[9] In addition to the total length of the fault system, the empirically constrained frequency distribution can be used to calculate the total amount of deformation accommodated by faults at slip-rate v. The extent of slip partitioning (as related to accommodating differential plate motion) is determined by the total amount of deformation accommodated by faults at slip-rate, v, as the product of the fault slip-rate and that length of the fault system at that slip-rate, $L(v)$. This quantity is the potency accumulation rate per unit depth, $\dot{P}_0^A$, and can be calculated in terms of the empirical frequency distribution as,

$$\dot{P}_0^A = \int_{v_1}^{v_2} N(v) v dv = \frac{c\left(v_2^{\theta+2} - v_1^{\theta+2}\right)}{\theta + 2}. \quad (2)$$

Note that the expressions both L and $\dot{P}_0^A$ are both finite and positive only for $\theta > -1$. Thus, in the parameter regime constrained by the estimated fault slip-rates, $-1.0 < \theta < -0.5$, the total length of the fault system may vary by two orders of magnitude while the total potency accumulation rate varies by approximately 40% (Figure 2a). This demonstrates that if the population of faults at slip-rates below currently detectable levels (<1 mm/yr) has the same statistical properties as those that have been sampled at greater slip-rates (>1 mm/yr), then the total potency accumulation rate remains finite and increases more slowly than the total fault system length. For example, as the proportion of slow slip-rate faults increases (e.g., θ decreases from -0.65 to -0.95) the length of the fault system increases by an order of magnitude while the potency accumulation rate only increases by ~20%.

[10] In southern California the maximum fault slip-rate is approximately 35 mm/yr along the central San Andreas

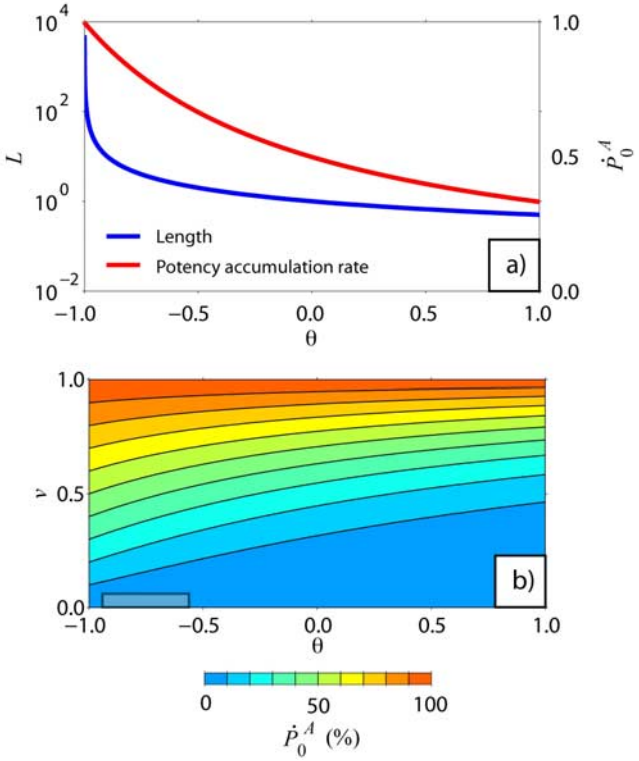

Figure 2. (a) Normalized ($c = 1$) fault system length (blue, logarithmic-scale) and potency accumulation rate (red, linear-scale) as a function of the power-law frequency distribution exponent, θ. Fault system length diverges as θ approaches -1 while the potency accumulation rate remains finite. (b) Percentage contribution to the total potency accumulation rate per unit depth, $\dot{P}_0^A$, from faults at a given slip-rate. Shaded region indicates the current limits of detection for faults in southern California. All fault slip-rates, ν, are normalized by the maximum observed slip-rate (~35 mm/yr).

[e.g., *Meade and Hager*, 2005; *Sieh and Jahns*, 1984], and the composite power-law exponent is -0.75 ± 0.18 (Figures 1c and 1d). Using these values and the derived relationship for the potency accumulation rate, equation (2) implies that ~97% of the motion between the Pacific and North American plates in southern California is accommodated on faults slipping at rates >1 mm/yr (Figure 2b). The remaining 1% of the total potency accumulation rate is accommodated on faults slipping below 1 mm/yr, which may be below currently detectable limits, and thus is difficult to explicitly parameterize as slip on discrete structures. While the length of the southern California fault system is eqi-partitioned between the <1, 1–10, and >10 mm/yr slip-rate regimes these, respectively, account for 1 ± 0.5%, 19 ± 4%, and 80 ± 5% of all plate boundary zone deformation. However, if a fault systems where characterized by a maximum fault slip-rate of ~2 mm/yr it would be significantly more difficult to identify the structures that accommodate most of the relative motion due the fact that a great fraction of the deformation budget would be accommodated by slip-rates <1 mm/yr. For a fault system with a maximum slip-rate of 2 mm/yr only 58 ± 5% of the potency accumulation would be accommodated on faults slipping at >1 mm/yr while the 42 ± 5% would remain on hard to identify faults moving at <1 mm/yr.

[11] We have considered the implications of a power-law distribution of fault slip-rates without a lower limit. This defines an end-member case in the sense that we allow very slow slip rate faults to contribute as much as possible to the potency accumulation rate budget, and also to the extent that we have ignored any mechanical constraints (e.g., characteristic fracture lengths) may impose physical limits on the minimum fault slip-rate. If a lower limit, $\nu_1 > 0$, is applied, then the role of low slip-rate faults in accommodating deformation is diminished by a factor of, $1 - (\nu_1/\nu_2)^{\theta+2}$, which ranges from 0 to 1 for $\theta > -2$.

4. Conclusions

[12] The empirically constrained power-law fault slip-rate distribution model described above suggests that if all faults slipping >1 mm/yr in upper crust of southern California can be identified, then they will provide a description of 97% of strain partitioning across the Pacific-North America plate boundary zone. This implies that an accurate mapping of these structures will identify the loci of 97% of all interseismic strain accumulation and thus coseismic strain release. At the same time, the remaining 3% of deformation is inferred to occur on a large number of very slow slip-rate faults still accumulate strain slowly and have the potential to generate large, though infrequent, earthquakes. The limit of a highly fractured crust ($\theta \rightarrow -1$) describes a continuum of faults where 10% the relative plate motion is accommodated on faults slipping at less than 10% of the fastest slip-rate in the fault system (Figure 2b). If faults systems at other highly active ($\nu_{max} > 10$ mm/yr) plate boundary zones behave in a statistically similar fashion, these results would suggest that upper crustal deformation is well described as localized on structures that are detectable with current geodetic and geologic techniques. Analyses of geologic and geodetic slip rate catalogs in other fault systems (e.g., India-Asia collision zone, Japan) may provide constraints on how the applicability of this model presented here and determine whether or not there is a universal frequency distribution for fault slip rates at plate boundary zones.

[13] **Acknowledgments.** Sinan Akciz, Michelle Cooke, and three anonymous reviewers of this manuscript and previous drafts provided thoughtful comments that led to a much improved paper. This research was supported by the Southern California Earthquake Center. SCEC is funded by NSF Cooperative Agreement EAR-0106924 and USGS Cooperative Agreement 02HQAG0008. The SCEC contribution number for this paper is 1130.

References

Argus, D. F., and R. G. Gordon (2001), Present tectonic motion across the Coast Ranges and San Andreas fault system in central California, *Geol. Soc. Am. Bull.*, *113*(12), 1580–1592.

Bennett, R. A., W. Rodi, and R. E. Reilinger (1996), Global positioning system constraints on fault slip rates in southern California and northern Baja, Mexico, *J. Geophys. Res.*, *101*(B10), 21,943–21,960.

Bennett, R. A., B. P. Wernicke, J. L. Davis, P. Elósegui, J. K. Snow, M. J. Abolins, M. A. House, G. L. Stirewalt, and D. A. Ferrill (1997), Global positioning system constraints on fault slip rates in the Death Valley region, California and Nevada, *Geophys. Res. Lett.*, *24*(23), 3073–3076.

Billen, M. I., and G. A. Houseman (2004), Lithospheric instability in obliquely convergent margins: San Gabriel Mountains, southern California, *J. Geophys. Res.*, *109*, B01404, doi:10.1029/2003JB002605.

Bourne, S. J., et al. (1998), The motion of crustal blocks driven by flow of the lower lithosphere and implications for slip rates of continental strike-slip faults, *Nature*, *391*(6668), 655–659.

Cowie, P. A., and C. H. Scholz (1992), Displacement length scaling relationship for faults - data synthesis and discussion, *J. Struct. Geol.*, *14*(10), 1149–1156.

DeMets, C., et al. (1990), Current plate motions, *Geophys. J. Int.*, *101*(2), 425–478.

DeMets, C., and T. H. Dixon (1999), New kinematic models for Pacific-North America motion from 3 Ma to present. I: Evidence for steady motion and biases in the NUVEL-1A model, *Geophys. Res. Lett.*, *26*(13), 1921–1924.

England, P., and D. McKenzie (1982), A thin viscous sheet model for continental deformation, *Geophys. J. R. Astron. Soc.*, *70*(2), 295–321.

England, P., and P. Molnar (1997), Active deformation of Asia: From kinematics to dynamics, *Science*, *278*(5338), 647–650.

Fay, N. P., and E. D. Humphreys (2005), Fault slip rates, effects of elastic heterogeneity on geodetic data, and the strength of the lower crust in the Salton Trough region, southern California, *J. Geophys. Res.*, *110*, B09401, doi:10.1029/2004JB003548.

Feigl, K. L., et al. (1993), Space geodetic measurement of crustal deformation in central and southern California, 1984–1992, *J. Geophys. Res.*, *98*(B12), 21,677–21,712.

Flesch, L. M., et al. (2000), Dynamics of the Pacific-North American plate boundary in the western United States, *Science*, *287*(5454), 834–836.

Friedrich, A. M., B. P. Wernicke, N. A. Niemi, R. A. Bennett, and J. L. Davis (2003), Comparison of geodetic and geologic data from the Wasatch region, Utah, and implications for the spectral character of Earth deformation at periods of 10 to 10 million years, *J. Geophys. Res.*, *108*(B4), 2199, doi:10.1029/2001JB000682.

Hanks, T. C., and W. H. Bakun (2002), A bilinear source-scaling model for M-log A observations of continental earthquakes, *Bull. Seismol. Soc. Am.*, *92*(5), 1841–1846.

Marrett, R., and R. W. Allmendinger (1992), Amount of extension on small faults - an example from the Viking Graben, *Geology*, *20*(1), 47–50.

McCaffrey, R. (2002), Crustal block rotations and plate coupling, in *Plate Boundary Zones*, *Geodyn. Ser.*, vol. 30, edited by S. Stein and J. Freymueller, pp. 101–122, AGU, Washington, D. C.

McCaffrey, R. (2005), Block kinematics of the Pacific–North America plate boundary in the southwestern United States from inversion of GPS, seismological, and geologic data, *J. Geophys. Res.*, *110*, B07401, doi:10.1029/2004JB003307.

McClusky, S. C., S. C. Bjornstad, B. H. Hager, R. W. King, B. J. Meade, M. M. Miller, F. C. Monastero, and B. J. Souter (2001), Present day kinematics of the Eastern California shear zone from a geodetically constrained block model, *Geophys. Res. Lett.*, *28*(17), 3369–3372.

Meade, B. J., and B. H. Hager (2005), Block models of crustal motion in southern California constrained by GPS measurements, *J. Geophys. Res.*, *110*, B03403, doi:10.1029/2004JB003209.

Minster, J. B., and T. H. Jordan (1987), Vector constraints on western United States deformation from space geodesy, neotectonics, and plate motions, *J. Geophys. Res.*, *92*(B6), 4798–4804.

Molnar, P. (1988), Continental tectonics in the aftermath of plate-tectonics, *Nature*, *335*(6186), 131–137.

Petersen, M. D., and S. G. Wesnousky (1994), Fault slip rates and earthquake histories for active faults in southern California, *Bull. Seismol. Soc. Am.*, *84*(5), 1608–1649.

Plesch, A., et al. (2007), Community Fault Model (CFM) for southern California, *Bull. Seismol. Soc. Am.*, in press.

Sauber, J., et al. (1994), Geodetic slip rate for the Eastern California Shear Zone and the recurrence time of Mojave Desert earthquakes, *Nature*, *367*(6460), 264–266.

Savage, J. C., and R. O. Burford (1973), Geodetic determination of relative plate motion in central California, *J. Geophys. Res.*, *78*(5), 832–845.

Shen-Tu, B., W. E. Holt, and A. J. Haines (1999), Deformation kinematics in the western United States determined from Quaternary fault slip rates and recent geodetic data, *J. Geophys. Res.*, *104*(B12), 28,927–28,955.

Sieh, K. E., and R. H. Jahns (1984), Holocene activity of the San Andreas Fault at Wallace Creek, California, *Geol. Soc. Am. Bull.*, *95*(8), 883–896.

Thatcher, W. (1995), Microplate versus continuum descriptions of active tectonic deformation, *J. Geophys. Res.*, *100*(B3), 3885–3894.

Weldon, R., and E. Humphreys (1986), A kinematic model of southern California, *Tectonics*, *5*(1), 33–48.

Wells, D. L., and K. J. Coppersmith (1994), New empirical relationships among magnitude, rupture length, rupture width, rupture area, and surface displacement, *Bull. Seismol. Soc. Am.*, *84*(4), 974–1002.

B. J. Meade, Department of Earth and Planetary Science, Harvard University, 20 Oxford Street, Cambridge, MA 02138, USA. (meade@fas.harvard.edu)